REGULAR PAPER

CrossMark

Temperature control of the growth of iron oxide nanoislands on Fe(001)

Toyo Kazu Yamada[1,2*], Yuki Sakaguchi[1], Lukas Gerhard[3], and Wulf Wulfhekel[3]

[1]Graduate School of Advanced Integration Science, Chiba University, Chiba 263-8522, Japan
[2]Molecular Chirality Research Center, Chiba University, Chiba 263-8522, Japan
[3]Institute of Nanotechnology, Karlsruhe Institute of Technology, 76021 Karlsruhe, Germany

*E-mail: toyoyamada@faculty.chiba-u.jp

The control of atomically flat interfaces between iron (Fe) and insulating oxide films, such as the Fe/MgO(001) interface, is crucial for tunnel-magnetoresistance (TMR) devices. However, the realization of an ideal atomically flat and clean interface is rather difficult since iron easily binds to impurities such as oxygen. Atomic step defects and iron oxide at the interface could reduce TMR. In this study, the oxidization of an atomically flat and clean Fe(001)-whisker single crystal at different substrate and annealing temperatures was investigated with an ultrahigh-vacuum scanning tunneling microscope (STM). Annealing up to a temperature of 850 K was required to obtain ordered and atomically flat Fe(001)-p(1×1)O terraces after the oxidization with the coexistence of Fe–O nanoislands (∼1 nm in height, ∼50 nm in size). We found that the growth of such nanoislands, which enhances interface roughness, strongly depends on the substrate temperature (T_S) during the oxidization. A T_S lower than 300 K reduces the coverage by the nanoislands to less than 10%. © 2016 The Japan Society of Applied Physics

1. Introduction

The bcc-Fe(001) surface has highly spin-polarized states.[1–4] With the combination of Fe(001) and a MgO(001) spacer, large tunnel-magnetoresistances (TMR) occurs. Thus, nowadays, the bcc-Fe/MgO(001) system is widely used as a TMR device for read heads, near-future magneto-random access memory (MRAM)[5,6] as well as electric-field-driven spintronic devices.[7] Experimental research on Fe/MgO and related tunnel junctions has mainly focused on the performance of full devices depending on the precise preparation technique and heuristic design rules have been developed. Despite all of these efforts, the giant TMR values of more than 1000% that were predicted independently by Butler et al. and Mathon and Umerski in 2001[8,9] have never been achieved experimentally. Recently, a novel exchange bias effect has been reported for the Fe/MgO interface, where antiferromagnetic Fe–O nanoclusters could pin the surrounding ferromagnetic Fe, reducing the TMR.[10] Several studies have indicated a partial oxidation of the topmost Fe layer[11,12] and it has been theoretically predicted that such oxidation will markedly reduce the spin filtering effect and thus the TMR ratio of the junction. However, experiments on an oxidized Fe surface have shown a much smaller change in TMR [120% at 300 K for Fe/p(1×1)-O/MgO/Fe(001)].[13–15] This indicates that the reason for the discrepancy between experiment and theory is still to be understood.

The growth of iron oxide on Fe films has been studied by scanning tunneling microscopy (STM) in ultrahigh-vacuum (UHV).[16,17] When Fe films (20–50 nm thick) on a MgO(001) substrate were oxidized (10^{-4} Pa) at 300 K with subsequent annealing at 925 K, an Fe(001)-p(1×1)O structure was formed on the surface,[15] while, when Fe was deposited on a MgO(001) substrate at 523 K under dosing O_2 (10^{-4} Pa), the Fe films transformed to Fe_3O_4(001) films,[17] i.e., several iron-oxide phases became energetically close.

In this study, a clean and atomically flat bcc-Fe(001) whisker grown via chemical vapor deposition (CVD) was used as a substrate.[1–4,18–20] We investigated different iron-oxide phases that form depending on the substrate temperature (T_S) during oxidization as well as different annealing
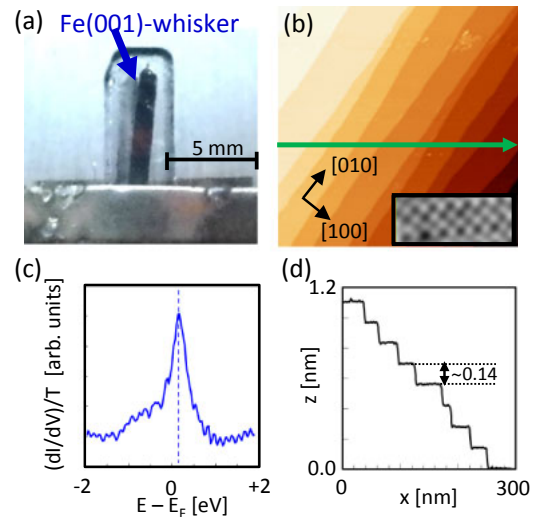
Fig. 1. (Color online) (a) Picture of the Fe whisker set in the Mo sample holder. (b) STM topographic image of the Fe(001) whisker surface after sputtering and annealing obtained at 300 K: $V_S = -1$ V, $I = 100$ pA, 300×300 nm². The inset shows an atomically resolved image. (c) dI/dV curve normalized by its fitted tunneling probability function obtained on Fe(001). (d) Line profile along the green arrow in (b).

temperatures after the oxidization. All experiments were performed with a home-built UHV-STM setup at 300 K.

2. Experimental methods

The home-built UHV-STM setup consists of preparation and analysis UHV chambers. In the preparation UHV chamber, the cleaning, oxidization, and annealing of the whisker were performed, and subsequently, without breaking UHV, the whisker was transferred to the analysis chamber and put into the STM setup. The temperature of the sample was examined using a pyrometer for $T > 550$ K and a thermocouple for $T < 550$ K.

We grew Fe(001) whiskers by a CVD process. One of the whiskers ($1 \times 1 \times 10$ mm³) was placed on a Mo sample holder [see Fig. 1(a)]. In the preparation UHV chamber, the Fe(001) whisker was first sputtered with Ar^+ ions at 870 K for 50 h, the sputtering was stopped, and, 5 min later, we stopped heating. Fe(001) was moved to the analysis UHV

chamber without breaking the UHV, and the Fe(001) surface was studied by STM. As shown in Fig. 1(b), atomically flat terraces were observed. The atomically resolved image in the inset in Fig. 1(b) shows a bcc Fe(001)-p(1×1) symmetry. A normalized $(dI/dV)/T$ curve obtained on the Fe(001) surface displays an LDOS peak at +0.2 eV above the Fermi energy in agreement with previous results.[1,3] A line profile along the arrow in Fig. 1(b) confirmed monolayer steps of ~0.14 nm, which corresponds to the literature value of a bcc-Fe(001) interlayer distance of 0.143 nm [see Fig. 1(d)].

We used tungsten (W) tips as STM probes, which were etched from commercial polycrystalline W wires with a KOH solution. The apex of the tips was examined using a scanning electron microscope (Technex. Tiny-SEM, ~10^{-3} Pa). Sharp tips were introduced into the STM setup and, in the preparation chamber, the tip apex was heated by electron bombardment (10–30 W: 500 V × 20–60 mA, 10 s)[21] to remove oxide from the apex. The cleaned tips were placed in the STM without breaking UHV.

All STM topographic images were obtained in the constant current mode (tunneling current feedback loop ON). We performed scanning tunneling spectroscopy (STS) measurements, in which the differential conductance dI/dV is first-order proportional to the sample local density of states (LDOS). During the spectroscopy, the tip–sample separation was fixed by switching off the feedback loop. The tunneling current was measured as a function of the sample bias voltage, typically from −1 to +1 V (I–V curve). The obtained I–V curves were numerically differentiated, and differential conductivity (dI/dV) curves were obtained and normalized by the tunneling matrix element in order to extract the sample LDOS even for large voltages.[22]

3. Results and discussion

This study focuses on the oxidization of the atomically flat and clean bcc-Fe(001) whisker (cf. Fig. 1) at different T_S during the oxidization and different annealing temperatures (T_A) after the oxidization.

Firstly, the Fe(001) whisker surface was oxidized at 300 K by dosing 2 L (1 L = 1.33×10^{-6} mbar s) of oxygen in the preparation chamber. Figures 2(a1) and 2(a2) show the surface, on which atomic steps and terraces of the Fe(001) whisker can still be observed. However, the entire surface seems to be roughened by oxygen exposure. A line profile along the arrow in Fig. 2(a2) shows a peak-to-peak corrugation of less than 100 pm on the terrace [cf. Fig. 2(b)]. A dI/dV curve obtained on this surface shows no peak, i.e., the Fe(001) d-state peak [Fig. 1(c)] at +0.2 eV was quenched [cf. Fig. 2(c)] after dosing 2 L of oxygen.

In the following, we examined how the oxidized surface changed with further annealing. Figures 2(d1) and 2(d2) show STM topographic images obtained after annealing to $T_A = 540$ K. As depicted in Fig. 2(d1), the original Fe(001) terraces are still observed. In Fig. 2(d2), in the same Fe(001) terrace, several layers are exposed. A line profile along the arrow in Fig. 2(d2) shows that the peak-to-peak corrugation increases to 250 pm [see Fig. 2(e)]. The dI/dV curve obtained on this surface [see Fig. 2(f)] is comparable to that in Fig. 2(c).

We further annealed the surface to $T_A = 740$ K. Then, the surface roughness increased and the original Fe(001) terraces
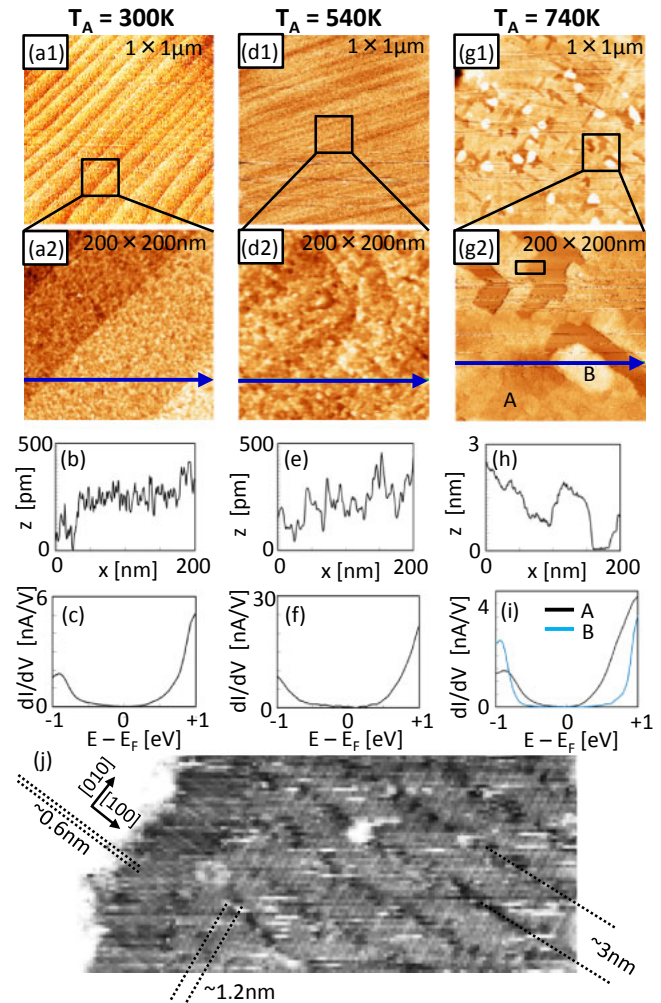
Fig. 2. (Color online) STM topographic images obtained on the oxidized-Fe(001) whisker single-crystal surface at 300 K in UHV. (a1, a2) STM images obtained after oxidization of the clean Fe(001) surface by dosing 2 L of O_2 at 300 K ($V_S = +2.5$ V, $I = 50$ pA). (b) Line profile along the arrow in (a2). (c) dI/dV curve obtained on the terrace in (a2) ($V_S = -1$ V, $I = 500$ pA). (d1, d2) STM images obtained after UHV annealing to $T_A = 540$ K (filament power: 2 W, 5 min) ($V_S = -2.5$ V, $I = 200$ pA). (e) Line profile along the arrow in (d2). (f) dI/dV curve obtained on the terrace in (d2) ($V_S = -2$ V, $I = 150$ pA). (g1, g2) STM images obtained after UHV annealing to $T_A = 740$ K (filament power: 3.5 W, 5 min) ($V_S = -2.5$ V, $I = 50$ pA). (h) Line profile along the arrow in (g2). (i) dI/dV curves obtained on the terrace (A) and the island (B) in (g2) ($V_S = -1$ V, $I = 500$ pA). (j) Nanostructures in the boxed area in (g2) (31×16 nm^2, $V_S = 2.1$ V, $I = 50$ pA).

completely disappeared. Instead, new terraces and islands appeared [cf. Figs. 2(g1) and 2(g2)].

A line profile along the arrow in Fig. 2(g2) shows that the islands have a typical height of ~1 nm with a width of ~50 nm [Fig. 2(h)], while the flat area has a roughness of 50–100 pm. The dI/dV curves obtained on the terrace [A in Fig. 2(g2)] and islands [B in Fig. 2(g2)] are different [Fig. 2(i)], i.e., they have different LDOSs, indicating that the islands and terrace are different Fe–O phases. On the terrace, we succeeded in obtaining a high-resolution image [Fig. 2(j)] whose area corresponds to the box in Fig. 2(g2). We observed two patterns: (1) one-dimensional (1D) lines along [100] with a periodicity of ~0.6 nm and (2) 1D lines along [010] with a periodicity of ~1.2 nm, which are separated every ~3 nm. Since similar patterns have been observed on Fe_3O_4(001) films grown on 4-nm-thick Fe buffer
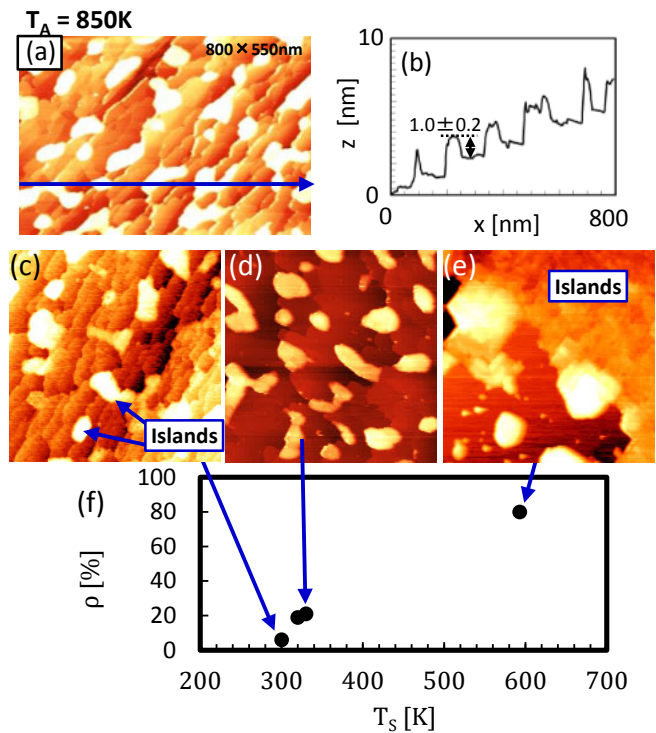
Fig. 3. (Color online) (a) STM topographic image of Fe(001) after dosing 2 L of O_2 at 300 K with subsequent annealing to $T_A = 850$ K (800×550 nm^2, $V_S = +1.5$ V, $I = 200$ pA). (b) Line profile along the arrow in (a). (c–e) STM topographic images of Fe(001) surfaces oxidized (2 L of O_2) at different T_S with subsequent annealing to $T_A = 850$ K: (c) $T_S = 300$ K, $V_S = +0.5$ V, $I = 50$ pA, and 500×500 nm^2. (d) $T_S = 330$ K, $V_S = +1.5$ V, $I = 100$ pA, and 500×500 nm^2. (e) $T_S = 590$ K, $V_S = -1.5$ V, $I = 100$ pA, and 400×400 nm^2. (f) Occupation of the surface by nanoislands as a function of the T_S during the oxidization.

layers UHV-annealed to 775 K,[23–25] the surface after 740 K annealing could be covered by a Fe$_3$O$_4$ film.

Annealing to $T_A = 850$ K leads to a rather marked change on the surface as shown in Fig. 3. On the surface, two different Fe–O phases coexist, i.e., atomically flat terraces and islands. The islands have a height of ∼1 nm and a width of ∼50 nm [see the line profile in Fig. 3(b)]. The atomically flat terraces have a typical width of ∼100 nm, i.e., the annealing temperature of 850 K is necessary to obtain an atomically flat surface.

We consider that the islands could be Fe–O nanoparticles that formed at the Fe/oxide interface as previously reported[10] and disturbed the atomically flat interface/surface. Therefore, we studied the island growth depending on the T_S during the oxidization. Results are shown in Figs. 3(c)–3(f); subsequent annealing to $T_A = 850$ K was always performed before STM measurements of the surface. When Fe(001) was oxidized at $T_S = 300$ K, $\rho \sim 10\%$ of the surface was covered by islands [Fig. 3(c)]; however, at $T_S = 340$ K, $\rho \sim 20\%$ of the surface was covered by islands [Fig. 3(d)], and further, at $T_S = 570$ K, islands covered $\rho = 70$–80% of the surface [Fig. 3(e)]. Figure 3(f) shows how much the surface was covered by islands [$\rho(\%)$] as a function of the T_S. These results show that island growth strongly depends on the T_S during oxidization. To prevent nanoisland growth and maintain an atomically flat interface, it is better to use a T_S lower than 300 K during the oxidization. We tested to expose the surface to up to 6 L of oxygen, but the island growth did

not change, indicating that 1–2 L of oxygen might be enough to cover the Fe(001) surface and additional oxygen desorbed during the annealing.

While the first layer of iron oxide forms as a continuous film, the growth mode changes upon the termination of the first layer. Then, the film atoms more strongly bind to each other than to the substrate, which leads to the growth of 3D islands. These results are in agreement with those of previous studies where the growth of a mixed iron layer on top of the FeO layer,[27] as well as that of oxide islands on top of the completed FeO layer,[15] was found.

We were interested in identifying the iron-oxide phases on the flat terraces and islands. Figure 4(a) shows the focused area, where one big island (area II) and atomically flat terraces (area I) are observed.

Firstly, we took an atomically resolved STM image on the flat terrace [the enlarged image in Fig. 4(a)], which shows the same symmetry as bcc-Fe(001). By comparison of our results with previously reported results,[15] we conclude that the flat terrace surface has a Fe(001)-p(1×1)O structure.

On the nanoislands (area II), flaky and rectangular structures were found. The line profile [cf. Fig. 4(b)] along the arrow in Fig. 4(a) shows that the distance between layers is ∼180 pm. Figure 4(c) shows an enlarged STM image obtained from an area with a rectangular structure. Bright spots that align along the [010] direction with a periodicity of ∼0.6 nm and along the [100] direction with a periodicity of ∼0.3 nm are observed, i.e, the spots form a p(2×1) structure with respect to the substrate bcc-Fe(001) lattice. When the same area as that in Fig. 4(c) was scanned with the STM tip, we frequently observed a different atomic structure as shown in Fig. 4(d), which has a similar lattice to the bcc-Fe(001) symmetry, i.e., the p(1×1) structure. Since these different observations can be obtained by a slight change at the tip apex, showing sublattices of different chemical species in metal-oxide films,[26] the observed p(2×1) and p(1×1) structures are probably alternating subterraces in iron oxide.

Figure 4(e) shows a sphere model. Black dots denote Fe atoms in a bcc(001) symmetry with a lattice constant of 287 pm. Grey circles are oxygen atoms adsorbed at hollow site positions on the Fe(001), corresponding to the p(1×1) structure. White circles align along the [010] direction with a periodicity of 574 pm (= 2 × 287 pm), corresponding to the p(2×1) structure.

It is well known in bulk that iron reacts with oxygen at 300–900 K via (1) $3/2\mathrm{Fe} + O_2 = 1/2\mathrm{Fe_3O_4}$, (2) $2\mathrm{Fe} + O_2 = 2\mathrm{FeO}$, (3) $6\mathrm{FeO} + O_2 = 2\mathrm{Fe_3O_4}$, and (4) $4\mathrm{Fe_3O_4} + O_2 = 6\mathrm{Fe_2O_3}$. Therefore, possible iron oxide structures are Fe$_3$O$_4$ (magnetite): cubic, $a = 0.8396$ nm, Fe$_{1-x}$O (wustite): cubic $a = 0.4302$ nm (Fe-rich), $a = 0.4275$ nm (Fe-poor), α-Fe$_2$O$_3$ (hematite): hcp $a = 0.5034$ nm, $c = 1.3752$ nm, and γ-Fe$_2$O$_3$ (maghemite): cubic or tetragonal $a = 0.834$ nm, $c = 2.501$ nm. Also, above 840 K, FeO is energetically stable. Since the obtained structures in our study are based on a bcc(001) symmetry, iron oxides with cubic structures, i.e., Fe$_3$O$_4$(001), Fe$_{1-x}$O(001), and γ-Fe$_2$O$_3$(001), could be fabricated.

Although Fe$_3$O$_4$ films similar to those in Figs. 2(g) and 2(j) were observed at $T_S = 550$ K with $T_A = 645$–775 K,[24] studies of iron-oxide films grown on a Fe(001) substrate at 300 K with higher annealing temperatures suggested the coexistence of FeO and γ-Fe$_2$O$_3$ phases.[27,28] By comparing
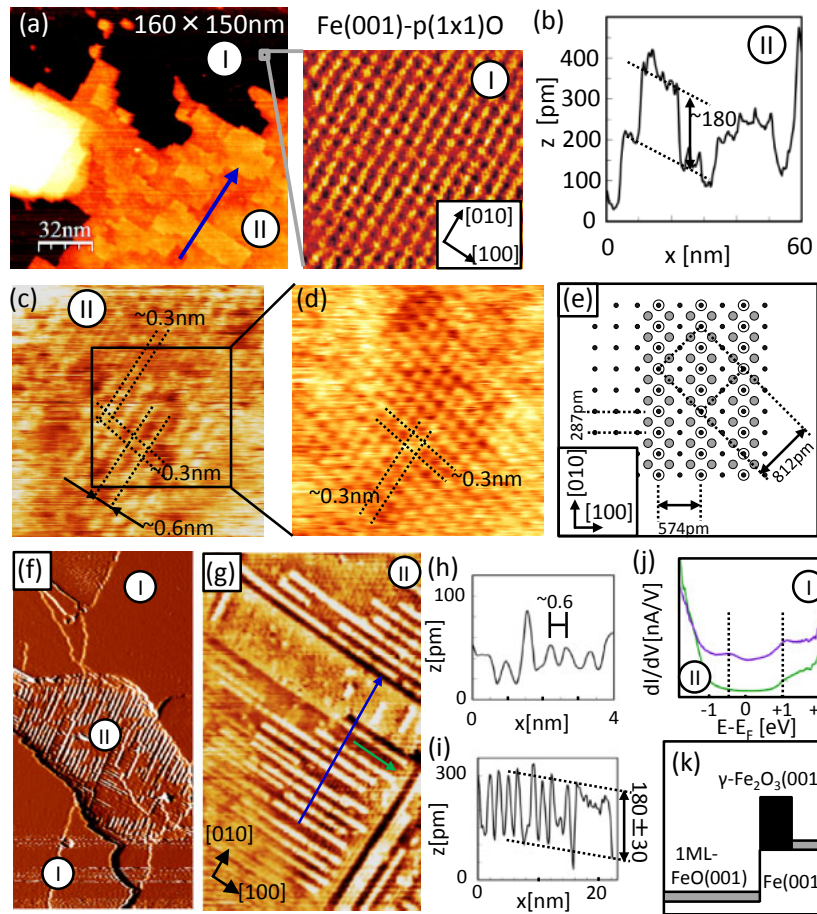
Fig. 4. (Color online) STM/STS measurements on Fe(001) surfaces oxidized (2 L of O_2) with subsequent annealing to $T_A = 850$ K. (a) STM image of the area including one large nanoisland (area II) and atomic terraces (area I). An enlarged image of area I shows an Fe(001)-p(1×1)O structure. (b) Line profile of area II along the arrow in (a). (c, d) Atomically resolved STM images obtained in area II [(c) 8 × 8 nm², $V_S = -9$ mV, and $I = 2$ nA; (d) 5 × 5 nm², $V_S = -15$ mV, and $I = 3$ nA]. (e) Sphere model of the obtained structures on a bcc-Fe(001) substrate. Black and grey dots denote Fe and oxygen atoms, respectively, and white circles denote (2×1). (f) STM current image (75 × 150 nm²) of the area including one large nanoisland (area II) and atomic terraces (area I). Step edges are enhanced. (g) High-resolution STM image on an island (area II). (h) and (i) Line profiles along the green and blue arrows in (g), respectively. (j) dI/dV curves obtained on the FeO terrace (purple line) and on the island (green line). (k) Model of the cross-sectional view of the obtained surface.

our STM images in Figs. 4(c) and 4(d) with those of γ-Fe_2O_3(001),[29] the experimentally obtained p(1×1) and p(2×1) structures could correspond to sublattices in γ-Fe_2O_3(001), i.e., p(2×1) octahedral Fe^{3+} and p(1×1) oxygen layers.

γ-Fe_2O_3 has a lattice constant of 834 pm, which fits the $2\sqrt{2} \times 287$ pm = 812 pm in a bcc-Fe(001) shown in Fig. 4(e), i.e., γ-Fe_2O_3 films on bcc-Fe(001) substrate display a small lattice mismatch of only ∼2.6%. The constant island height of ∼1 nm is similar to the lattice constant of γ-Fe_2O_3.

Figure 4(f) shows another island on the same surface as that in Fig. 4(a). This image was taken in the constant height mode, and the current map emphasizes step edges. In this imaging mode, 1D lines are clearly observed. Figure 4(g) shows an enlarged image. On terraces on the island in Fig. 4(g), 1D lines along the [010] direction, whose periodicity is ∼0.6 nm [see the line profile in Fig. 4(h) along the green arrow in Fig. 4(g)], can be seen corresponding to the (2×1) structure in Fig. 4(c). On top of the (2×1) structure, the next layer starts to grow along the [100] direction. The distance between layers is ∼180 pm [see the line profile in Fig. 4(i) along the blue arrow in Fig. 4(g)], which is the same

as that in Fig. 4(b), indicating that the stacking structure seems to be the same for all nanoislands.

Furthermore, we performed STS measurements to determine the LDOS. Figure 4(j) shows dI/dV curves obtained on the Fe(001)-p(1×1)O flat terrace (area I, purple line) and γ-Fe_2O_3(001)-like nanoislands (area II, green line). The FeO terrace has peaks at −0.5 and +1.0 eV, which are in good agreement with Ref. 30. However, on the islands, the −0.5 peak seems to shift below −1 eV, while the +1 eV peak is suppressed.

From these studies, we can conclude the following. At $T_S \sim 550$ K, mainly Fe_3O_4 films are grown. Annealing to 850 K might change the structure from Fe_3O_4 to Fe_2O_3, but with a very low possibility to generate FeO. On the other hand, when we oxidize Fe(001) at $T_S = 300$ K with subsequent annealing, different iron-oxide films are grown at different T_A: $T_A \leq 540$ K amorphous films, $T_A = 740$ K Fe_3O_4(001)-like films, and $T_A = 850$ K atomically flat FeO(001) films and γ-Fe_2O_3 three-dimensional nanoislands. Iron oxides, such as Fe_3O_4 and Fe_2O_3, are ferrimagnets. If iron oxide islands grow at iron/oxide film interfaces, owing to an exchange bias effect, the islands could pin the surrounding ferromagnetic Fe and decrease TMR.

4. Conclusions

An atomically flat and clean bcc-Fe(001) whisker single crystal surface was oxidized (2 L) in UHV. The produced iron oxide was studied as a function of the T_S during the oxidation and the annealing temperature after the oxidation. The annealing temperature of 850 K is necessary to obtain an ordered atomically flat Fe(001)-p(1×1)O surface with Fe–O nanoislands. The growth of islands was found to be controlled by the T_S during oxidation. By setting the T_S lower than 300 K during oxidization, the number of islands on the surface could be reduced to less than 10%. However, at substrate temperatures higher than 500 K, most of the surface (70–80%) was covered by Fe–O nanoislands. The island growth was not affected by the oxygen dose between 1 and 6 L. These experimental findings are important in producing an atomically flat ordered Fe/oxide interface.

1) J. A. Stroscio, D. T. Pierce, A. Davis, and R. J. Celotta, Phys. Rev. Lett. **75**, 2960 (1995).
2) M. Klaua, D. Ullmann, J. Barthel, W. Wulfhekel, J. Kirschner, R. Urban, T. L. Monchesky, A. Enders, J. F. Cochran, and B. Heinrich, Phys. Rev. B **64**, 134411 (2001).
3) M. M. J. Bischoff, T. K. Yamada, C. M. Fang, R. A. de Groot, and H. van Kempen, Phys. Rev. B **68**, 045422 (2003).
4) S. Nakashima, Y. Yamagishi, K. Oiso, and T. K. Yamada, Jpn. J. Appl. Phys. **52**, 110115 (2013).
5) M. Przybylski, J. Gradowski, F. Zavaliche, W. Wulfhekel, R. Scholz, and J. Kirschner, J. Phys. D **35**, 1821 (2002).
6) S. Yuasa, T. Nagahama, A. Fukushima, Y. Suzuki, and K. Ando, Nat. Mater. **3**, 868 (2004).
7) T. Maruyama, Y. Shiota, T. Nozaki, K. Ohta, N. Toda, M. Mizuguchi, A. A. Tulapurkar, T. Shinjo, M. Shiraishi, S. Mizukami, Y. Ando, and Y. Suzuki, Nat. Nanotechnol. **4**, 158 (2009).
8) W. Butler, X.-G. Zhang, T. Schulthess, and J. MacLaren, Phys. Rev. B **63**, 054416 (2001).
9) J. Mathon and A. Umerski, Phys. Rev. B **63**, 220403 (2001).
10) Y. Fan, K. J. Smith, G. Lupke, T. Hanbicki, R. Goswami, C. H. Li, H. B. Zhao, and B. T. Jonker, Nat. Nanotechnol. **8**, 438 (2013).
11) D. Telesca, B. Sinkovic, S.-H. Yang, and S. Parkin, J. Electron Spectrosc. Relat. Phenom. **185**, 133 (2012).
12) S. Kamali, C. L. Zha, Y. Yoda, and J. Akerman, J. Phys.: Condens. Matter **26**, 026004 (2014).
13) P.-J. Zermatten, F. Bonell, S. Andrieu, M. Chshiev, C. Tiusan, A. Schuhl, and G. Gaudin, Appl. Phys. Express **5**, 023001 (2012).
14) F. Zavaliche, M. Przybylski, W. Wulfhekel, J. Gradowski, R. Scholz, and J. Kirschner, Surf. Sci. **507–510**, 560 (2002).
15) F. Bonell, S. Andrieu, A. M. Bataille, C. Tiusan, and G. Lengaigne, Phys. Rev. B **79**, 224405 (2009).
16) A. Tange, C. L. Gao, B. Yu. Yavorsky, I. V. Maznichenko, A. Etz, A. Ernst, W. Hergert, I. Mertig, W. Wulfhekel, and J. Kirschner, Phys. Rev. B **81**, 195410 (2010).
17) S. Hiura, A. Ikeuchi, S. Shirini, A. Subagyo, and K. Sueoka, Phys. Rev. B **91**, 205411 (2015).
18) T. K. Yamada, M. M. J. Bischoff, T. Mizoguchi, and H. van Kempen, Surf. Sci. **516**, 179 (2002).
19) T. K. Yamada, M. M. J. Bischoff, G. M. M. Heijnen, T. Mizoguchi, and H. van Kempen, Phys. Rev. Lett. **90**, 056803 (2003).
20) T. K. Yamada, H. Tamura, M. Shishido, T. Irisawa, and T. Mizoguchi, Surf. Sci. **603**, 315 (2009).
21) T. K. Yamada, T. Abe, N. M. K. Nazriq, and T. Irisawa, Rev. Sci. Instrum. **87**, 033703 (2016).
22) V. A. Ukraintsev, Phys. Rev. B **53**, 11176 (1996).
23) G. Maris, O. Shklyarevskii, L. Jdira, J. G. H. Hermsen, and S. Speller, Surf. Sci. **600**, 5084 (2006).
24) E. M. Davis, K. Zhang, Y. Cui, H. Kuhlenbeck, S. Shaikhutdinov, and H.-J. Freund, Surf. Sci. **636**, 42 (2015).
25) R. Bliem, E. McDermott, P. Ferst, M. Setvin, O. Gamba, J. Pavelec, M. A. Schneider, M. Schmid, U. Diebold, P. Blaha, L. Hammer, and G. S. Parkinson, Science **346**, 1215 (2014).
26) B. Stanka, W. Hebenstreit, U. Diebold, and S. A. Chambers, Surf. Sci. **448**, 49 (2000).
27) S. J. Roosendaal, B. van Asselen, J. W. Elsenaar, A. M. Vredenberg, and F. H. P. M. Hadraken, Surf. Sci. **442**, 329 (1999).
28) S. J. Roosendaal, A. M. Vredenberg, and F. H. P. M. Hadraken, Phys. Rev. Lett. **84**, 3366 (2000).
29) S. A. Chambers and S. A. Joyce, Surf. Sci. **420**, 111 (1999).
30) F. Donati, P. Sessi, S. Achilli, A. Li Bassi, M. Passoni, C. S. Casari, C. E. Bottani, A. Brambilla, A. Picone, M. Finazzi, L. Duo, M. I. Trioni, and F. Ciccacci, Phys. Rev. B **79**, 195430 (2009).